16th World Conference on Earthquake, 16WCEE 2017

Santiago Chile, January 9th to 13th 2017

Paper N° 643 (Abstract ID)

Registration Code: S-N1463106680

SEISMIC PERFORMANCE OF PRECAST PRESTRESSED CONCRETE FRAME ASSEMBLED BY UNBONDED TENDON WITH CAST-IN-PLACE RC SLAB

K. Jin(1), S. Song(2), K. Kitayama(3) and K. Kanemoto(4)

(1) *Ph.D., Research Assistant Professor, Tokyo Metropolitan University, Japan, kwjin@tmu.ac.jp*
(2) *Ph.D. Candidate, Tokyo Metropolitan University, Japan, song-sunghoon@ed.tmu.ac.jp*
(3) *Ph.D. Professor, Tokyo Metropolitan University, Japan, kitak@tmu.ac.jp*
(4) *Master of Eng. Senior Research Engineer, Institute of Technology, Shimizu Corporation, Japan, kanemoto@shimz.co.jp*

Abstract

In this study, the seismic capacity of an 'unbonded PCaPC' structure, a precast prestressed concrete frame assembled by post-tensioning unbonded tendons, with cast-in-place RC slabs is investigated. For this purpose, cruciform unbonded PCaPC subassemblages, where the beam flexural failure preceded, were designed, and their reversed cyclic loading tests were carried out. Herein, the main parameter was set to be the partial cut-off of longitudinal bars in the RC slab, which were arranged around the column, since it was considered to affect the damage condition of the slab. From the experiment results, the flexural behavior of unbonded PCaPC beams with RC slabs, including damage patterns, hysteretic characteristics, residual crack opening widths and energy dissipating capacity, is investigated at their positive and negative loading. In addition, some of those test results are compared with the prediction based on a new guideline for seismic performance evaluation of prestressed concrete buildings, recently proposed by the Architectural Institute of Japan. Different limit states of the beam, classified as 'service limit', 'first restorable limit', 'second restorable limit' and 'safety limit', which are determined from the damage level of tendons and concrete, as well as from the residual deflection and crack widths, are also discussed based on the guideline.

Keywords: precast prestressed concrete structure; post-tensioning unbonded tendon; cast-in-place RC slab; prestress ratio; seismic performance

1. Introduction

A precast prestressed concrete structure consisting of precast concrete members assembled by post-tensioning unbonded tendons, called an 'unbonded PCaPC' frame, is one of the latest construction methods to build moment-resisting frames, and it has several structural benefits[1]. In this method, a precast prestressed beam member damaged due to an earthquake can be replaced more easily than other construction methods, since the grouting work is eliminated, which can also make the labor-saving possible. In addition, because of the unbonded tendon, damaged areas are localized at the beam-column interface causing a remarkable crack opening, so the damage-control is possible. However, there is insufficient research regarding seismic performance and flexural behavior of unbonded PCaPC frames with reinforced concrete (RC) slabs, which are casted in a site to actual buildings. If a beam has a slab, the seismic behavior, at its positive and negative loading, can be somewhat different because of the slab and the different prestress ratio (λ)[2], where λ is defined as the moment contribution of tendons to the ultimate flexural capacity of a beam section. Besides, against the earthquake excitation, the unbonded PCaPC frame is designed as a strong column-weak beam system; therefore, the seismic capacity evaluation of unbonded PCaPC beams with RC slabs is necessary to mitigate the earthquake damage for these buildings.

For this purpose, in this study, cruciform unbonded PCaPC subassemblages with RC slabs, where the beam flexural failure preceded, were designed, and their reversed cyclic loading tests were carried out. Herein, the main parameter was set to be the partial cut-off of longitudinal bars in the RC slab, which were arranged around the column, since it was considered to affect the damage condition of the slab. From the experiment results, the flexural behavior of unbonded PCaPC beams with RC slabs, including damage patterns, hysteretic characteristics, residual crack opening widths and energy dissipating capacity, is investigated at their positive and negative loading; additionally, some of those results are compared with the prediction based on a new guideline for seismic performance evaluation of prestressed concrete buildings[2], recently proposed by the Architectural Institute of Japan. Different limit states of the beam, classified as 'service limit', 'first restorable limit', 'second restorable limit' and 'safety limit', which are determined from the damage level of tendons and concrete, as well as from the residual deflection and crack widths, are also discussed based on the guideline.

2. Experiment outline

2.1 Specimens and experiment parameters

Fig. 1 shows the configurations, section dimensions and reinforcement details of the specimens. The properties of specimens and materials are summarized in Table 1 and 2. Two half-scaled cruciform subassemblage specimens with cast-in-place RC slabs were fabricated, which represent the regions from mid-column height below the joint to mid-column height above the joint and mid-span to mid-span of beams on both sides of the joint. The section dimensions, reinforcement and tendons in columns and beams are the same for both specimens. The column size with a square cross section was 350mm by 350mm, and the beam section had a width of 250 mm and a depth of 400mm. The length from the center of columns to the roller support of beam ends was 1,600mm. The height from the center of beams to the loading point on the top of the column or to the bottom support was 1,415mm. Post-tensioning unbonded tendons of ϕ21 were employed for the beam, and the concrete compressive strength was around 70MPa in all members. In order to investigate the effect of the cast-in-place RC slab, as well as its effective width, the slab width (975mm) was set to be 0.3 times the beam span, and the longitudinal bar of D6 was used. Herein, the main parameter was set to be the partial cut-off of slab longitudinal bars around the column, as can be seen in Fig. 1, since it was considered to affect the damage condition of the slab. The prestress ratio (λ) at the positive loading is 1.0 in both specimens. On the other hand, λ at the negative loading is 0.59 in specimen PCJ01S, and that of PCJ02S is 0.69 due to the cut-offed slab reinforcement.

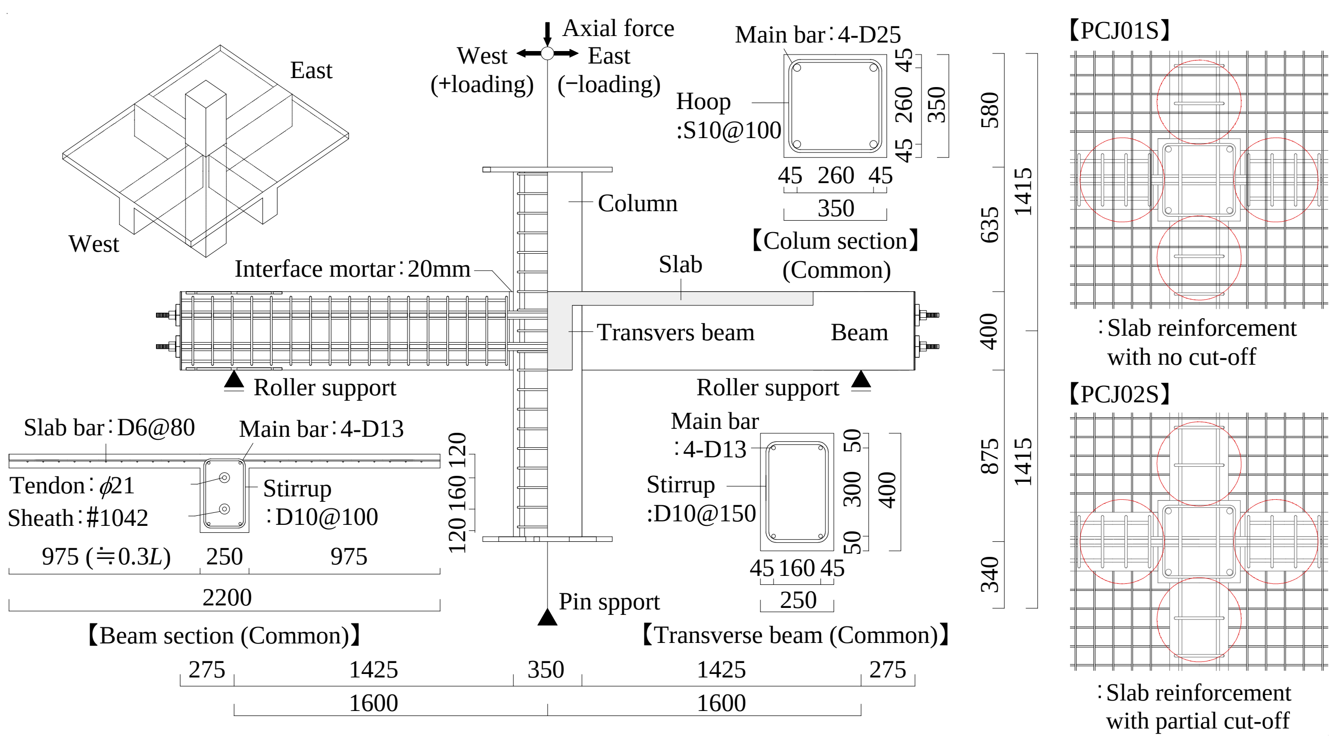

Fig. 1 – Specimen details

Table 1 – Specimen properties

Specimen			PCJ01S	PCJ02S
Beam	Section (b×D)		250mm×400mm	
	Tendon		2-φ21 (SBPR 930/1230)	
	Initial prestress force		273kN for a tendon	
	Prestress ratio (λ)*1)	Positive loading	1.0	
		Negative loading	0.59	0.69
	Longitudinal bar		4-D13(SD295A)	
	Stirrup		D10@100(SD295A)	
Column	Section (b×H)		350mm×350mm	
	Longitudinal bar		4-D25(SD390)	
	Hoop		S10@100(KSS785)	
	Axis compressive load		860kN	
Slab	Width×Thickness		2200mm×70mm	
	Longitudinal bar		D6@80(SD295A)	
	Numbers of longitudinal bars with no cut-off		22	14
Column-to-beam flexural strength			1.67	1.83

*1) $\lambda=M_p/(M_p+M_r)$; where M_p: moment contribution of tendon to ultimate beam flexural capacity, M_r: moment contribution of slab longitudinal bars to ultimate beam flexural capacity

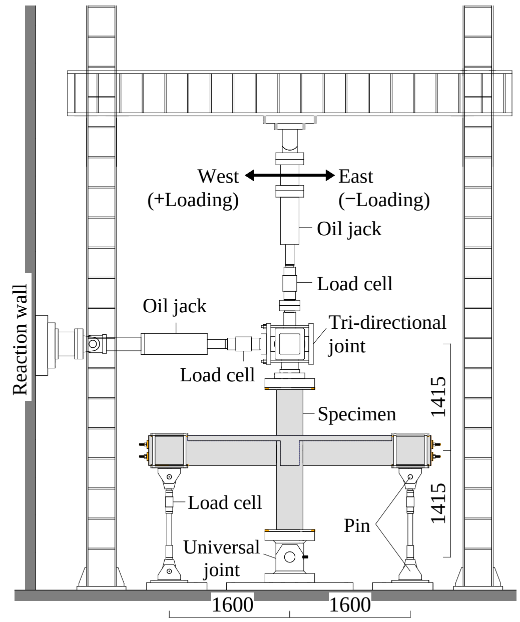

Fig. 2 – Test setup

Table 2 – Material properties

Concrete	PCJ01S			PCJ02S		
	Column・Beam	Slab	Interface mortar	Column・Beam	Slab	Interface mortar
Compressive strength	68.0MPa	65.2MPa	91.5MPa	71.2MPa	71.0MPa	108.9MPa
Split tensile strength	2.6MPa	2.7MPa	2.9MPa	3.0MPa	2.1MPa	4.3MPa

Bar／Tendon	Diameter	Standard	Yielding strength	Tensile strength	Yield strain	Elastic-limit strain*2)
Bar	D6*1)	SD295A	358MPa	525MPa	0.37%	-
	D10	SD295A	364MPa	509MPa	0.18%	-
	S10*1)	KSS785	969MPa	112 MPa	0.74%	0.43%
	D19	SD490	529MPa	715MPa	0.26%	-
	D25	SD390	457MPa	653MPa	0.22%	-
Tendon*1)	φ21	SBPR 930/1230	1006MPa	1124MPa	0.70%	0.44%

*1) Yield strength and strain were determined by 0.2% offset method.
*2) Elastic-limit strain was determined by 0.01% offset method.

In both specimens, RC columns and beams, assembled by post-tensioning unbonded tendons, were fabricated separately; hence, beam longitudinal bars were terminated at the column face without passing through the joints. The beam and column members were then connected through interface mortar with a width of 20mm, and, after the mortar had sufficient strength, unbonded tendons were post-tensioned up to 80% of their yield strength. Hereafter, the reinforcing bars were arranged and the concrete was cast in the slabs. The column-to-beam flexural strength (moment capacity) ratio[3] exceeded about 1.7 in both specimens, and the specimens were designed to form the beam collapse mechanism prior to the column yielding.

2.2 Loading program and instrumentation

The loading systems of the specimens are shown in Fig. 2. The beam ends were supported by horizontal rollers, while the bottom of the column was supported by a universal joint. The horizontal and constant axial compressive load were applied to the top of the column through tri-directional actuators. The actuator orthogonal to the horizontal loading direction was set to prevent out-of-plane behavior of specimens. All specimens were controlled by a story drift angle (R), defined as the story drift (δ) divided by column height (2,830mm). Two loading cycles for R of 0.125, 0.25, 0.5, 0.75, 1.0, 1.5, 2.0, 3.0 and 4.0% were imposed on each specimen. The horizontal force applied to the top of the column, the column axial load and the beam shear force were measured by load-cells. The story drift and deflections of each member were measured by displacement transducers. The strains of tendons, as well as those of beam and column reinforcement, were measured by strain gauges.

3. Experiment result

3.1 Load-deformation relationship

The story shear force (Q)-story drift angle (R) relations in the specimens are shown in Fig. 3. The story shear force was obtained from the moment equilibrium with the measured beam shear force. The story shear strength calculated from the ultimate flexural capacity of the beam[2] is also shown in Fig. 3, where the slab longitudinal bars passing around the column were only considered in the strength calculation at the negative loading.

In both specimens, no yielding of reinforcement in beams, columns and joint panels was observed, but the yielding of the slab reinforcement, which was closest to the column, initiated from a story drift angle of 0.4%. The tensile strain of tendons in both specimens reached their elastic-limit almost at the same time, although they did not yield. In specimen PCJ02S, 36% of slab reinforcing bars were partially cut-offed around the column, while its concrete compressive strength was about 10% higher than that of specimen PCJ01S. Hence, relatively lower strength was expected in specimen PCJ02S, but the maximum story shear force was found to be almost similar to that of specimen PCJ01S. Even though the slab longitudinal bars in specimen PCJ02S were partially cut-offed around the column, 8.3d (d: slab bar diameter) of their length were embedded inside the column face (Fig. 1); therefore, most of these reinforcement contributed to the strength increase of the beam at the negative loading. The maximum story shear forces from experiment results ranged from 0.98 to 1.1 times the calculations in both specimens, which showed good agreement.

The beam shear force (Q_b)-beam deflection angle (R_b) relationships in both specimens are shown in Fig. 4.

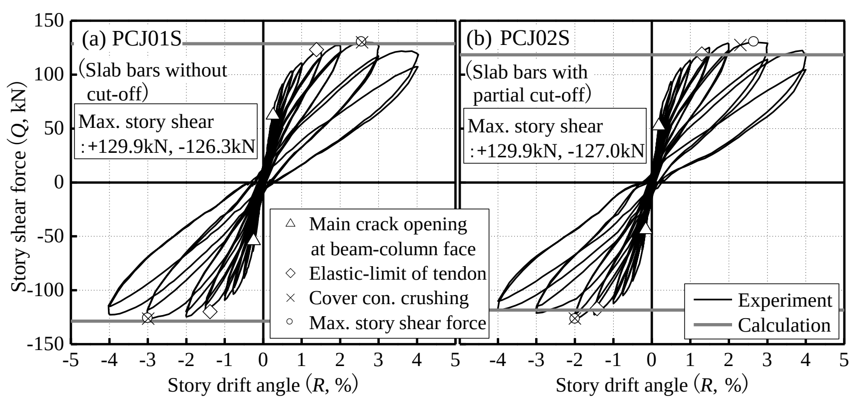

Fig. 3 – Story shear force-story drift angle relation

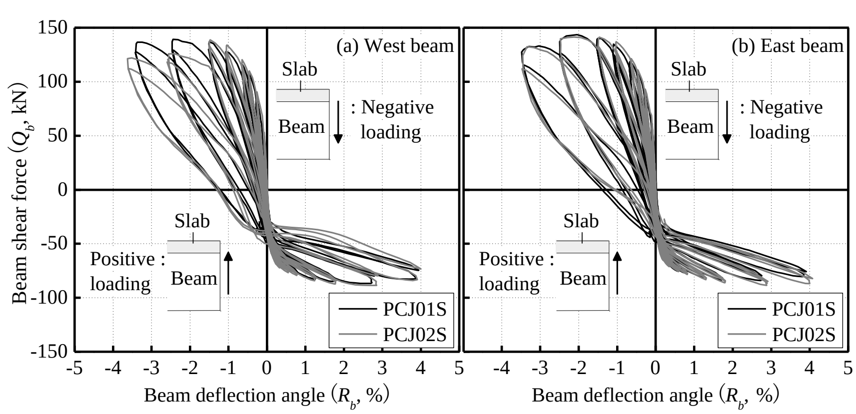

Fig. 4 – Beam shear force-beam deflection angle relation

As shown in the figure, hysteresis characteristics, energy absorbing capacity, peak and residual deflections in a T-shaped beam were found to be totally different at its positive and negative loading, due to slab reinforcement and different prestress ratios (λ). Especially, the residual beam deflection at the negative loading became larger, while that of positive loading remained nearly zero. It should be noted that, in the west beam of specimen PCJ02S, the beam shear force, at the negative loading, was slightly lower than that of specimen PCJ01 (Fig. 4 (a)). In contrast, the beam shear forces were almost identical in the east beams of both specimens. Therefore, some of cut-offed slab reinforcement in the west beam, which were embedded inside the column face and contributing to the strength increase, are suspected to be pulled out, as the beam deflection grows, which will be explained in next chapter. The equivalent effective slab widths and different behavior of beams at the positive and the negative loading, which includes residual beam deflections, equivalent viscous damping ratios and different limit states, will be also discussed in the next chapter in more detail.

3.2 Crack patterns and story drift contribution

Fig. 5 shows the crack patterns in both specimens after a story drift angle of 4%, where the spall-off of cover concrete are marked as shaded regions. In both specimens, the main crack opening at beam-column interfaces and the flexural crack in columns occurred at a drift angle of 0.25%. The flexural cracks in the slab were also developed at this drift angle. The main crack in the beam concentrated and opened at its critical section at both the positive and negative loadings. The wide propagation of cracks in the slab were observed along its axial direction, as the story drift increased, but lesser cracks expanded at the bottom of beam members, which was attributed to different prestress ratios (λ) at the positive and the negative loading. The cover concrete at beam critical sections began to spall-off at the maximum story shear force, and the beam concrete crushing mainly resulted in the strength degradation in both specimens. When a negative loading applies to a T-shaped beam, the distance from the extreme compression fiber to the neutral axis tends to be larger than that of a positive loading, so the concrete damage at the bottom of beam critical sections became more severe. The neutral axis at the positive and the negative loading will be investigated from the experiment results in the next chapter.

As can be seen in Fig. 5, there were slightly lesser cracks in the slab of specimen PCJ02S, which had partial cut-off of slab reinforcement. The intent of the cut-offed slab reinforcement was to reduce the transmission of tensile forces to the slab concrete so that the cracks could be restrained. However, those cut-offed slab reinforcing bars were embedded inside the column face; also, although some cut-offed slab bars were expected to be pulled-out with the growth of beam deformation, as mentioned above, it occurred at rather large deformation stage. Accordingly, the reasonable verification for the effects of those cut-offed slab bars on the damage condition is considered to be somewhat difficult. The maximum crack widths at beam-column interfaces were approximately 13 to 14.5mm and 2.5mm at the peak and the residual beam deflection angle in both specimens, which were almost similar, and obvious differences were not found.

The contribution of deformations by beams, columns and a joint panel to the story drift was calculated in both specimens, as shown in Fig. 6. In the figure, the contribution by the joint panel was assumed to be the difference between the directly measured story drift and the contribution by measured deflection of beams and columns. Each contribution by beams, columns and the joint panel was found almost similar in both specimen.

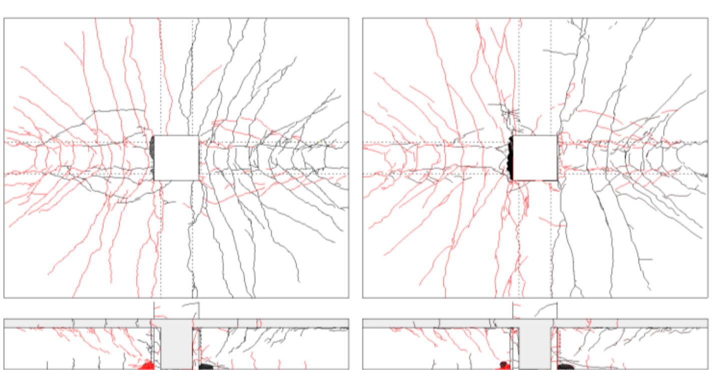
(a)PCJ01S (b)PCJ02S

Fig. 5 – Crack pattern

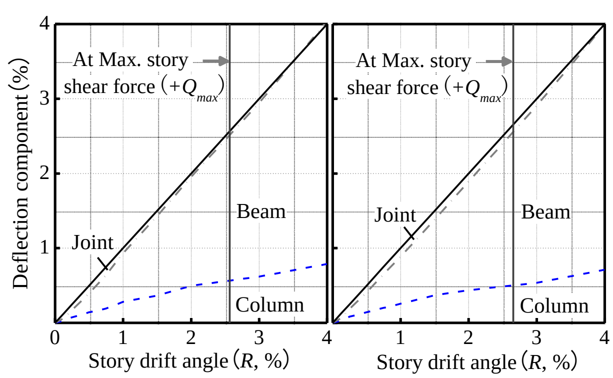

(a) PCJ01S (b) PCJ02S

Fig. 6 – Deflection component of story drift

The contribution by beams exceeded 70% of the total story drift at the maximum story shear force (Q_{max}). Judging from the maximum story shear force by experiment and calculation results, crack patterns and the story drift contribution, both specimens failed in beam flexure.

4. Discussions

4.1 Equivalent effective slab width

The equivalent effective slab widths ($b_{a,eq}$) on beam bending moment in both specimens were investigated and shown in Fig. 7. In this study, the tensile force of the slab reinforcement, at beam critical sections with the negative loading, was first calculated from its strain data. Herein, the stress (σ_{ti})-strain (ε_{ti}) relation of the slab bar was set to be bi-linear, and its tensile stress was assumed to be yield stress when its strain value exceeded the yielding strain. The obtained tensile force was then compared with the yielding strength of total slab reinforcing bars, and $b_{a,eq}$ was calculated based on their ratios, as shown in Eq. (1)[4].

$$b_{a,eq} \cdot t \cdot p_t = A_{ef} = \sum_{i=1}^{n} (\sigma_{ti} \cdot A_t) / \sigma_y \tag{1}$$

where, t is the slab thickness, p_t is the slab reinforcement ratio, A_{ef} is the effective area of the slab reinforcement, n is the total numbers of slab reinforcement, σ_{ti} is the tensile force of each slab reinforcement obtained from strain data during the experiment, A_t is the section area of a slab reinforcing bar and σ_y is the yielding strength of the slab reinforcement.

The width $b_{a,eq}$ in both specimens, which is the average value in the west and the east beam, gradually increased as the beam deflection grew, and they were found almost similar before the maximum strength of the beam. As mentioned earlier, some of slab bars were partially cut-offed around the column in specimen PCJ02S, but 8.3d (d: reinforcement diameter) of their length was embedded inside the column face. Accordingly, those slab bars were able to resist the tensile force, which was also confirmed from their strain data, and it attributed to the similar increasing tendency of $b_{a,eq}$ in both specimens. Nevertheless, with the growth of beam deformation, the tensile strain no more increased in some cut-offed slab bars, at the negative loading of the west beam, when the shear force was applying to the beam. Therefore, those reinforcing bars were considered to be pulled out, and $b_{a,eq}$ of specimen PCJ02S resulted in a slight decrease after the maximum strength, which also affected the strength degradation of the beam (Fig. 4 (a)). From Fig. 7, $b_{a,eq}$ exceeded 0.1 and 0.2 times the beam span at beam deflection angles of 0.4% and 1.2%, respectively, and reached almost whole slab width at the end of the test in specimen PCJ01S.

4.2 Distance from extreme compression fiber to neutral axis at beam critical section

In a T-shaped beam, the distance (x_n) from the extreme compressive fiber to the neutral axis becomes different at the positive and the negative loading due to the slab and its reinforcement, which can also affect the beam concrete damage. Therefore, x_n at the beam critical section was investigated in both specimens, and the

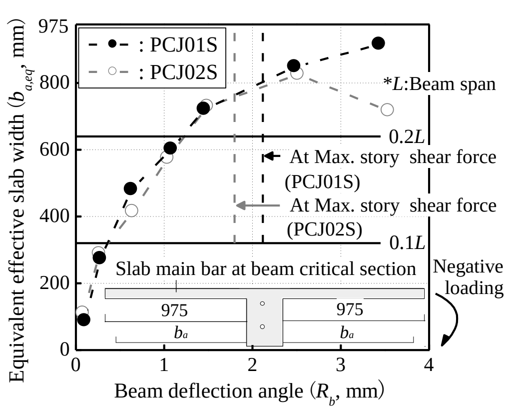

Fig. 7 – Equivalent effective slab width (Avg. in west and east beams)

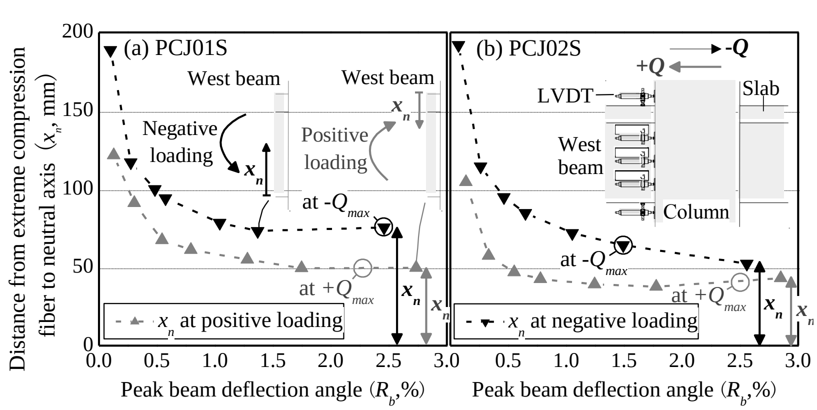

Fig. 8 – Distance from extreme compression fiber to neutral axis (West beam)

relationship between x_n and the peak beam deflection angle (R_b) is plotted in Fig. 8. In this study, the experiment data measured from five displacement transducers, which were attached adjacent to the west beam-column interface (50mm apart from the column face), was interpolated to determine x_n (Fig. 8 (b)). As shown in Fig. 8, the value of x_n at both the positive and negative loadings abruptly dropped as the crack opening occurred at the beam-column interface, but x_n gradually decreased with the increase of beam deformation. In addition, the distance x_n tended to be almost constant before the maximum story shear force ($\pm Q_{max}$), except for the specimen PCJ02S at its negative loading. In specimen PCJ02S, as mentioned earlier, some of cut-offed slab reinforcement did not resist the tensile force after the maximum strength, so x_n is considered to be smaller. It should be also noted that the severe concrete damage, developed at the bottom side of beam critical sections, resulted from the larger x_n at the negative loading.

4.3 Residual beam deflection ratio

The residual deflection ratio (r_b) of beam members, defined as the ratio of the residual beam deflection at the unloading stage to the beam deflection at the peak loading, was investigated from the experiment results. The relationship between r_b and the beam deflection angle (R_b), recorded at each peak loading, is shown in Fig. 9, where r_b and R_b are the average values in the west and the east beam. In general, the larger the prestress ratio (λ) is, the smaller r_b is, which was also observed in this test. The value of r_b was slightly lower in specimen PCJ02S, but distinctive difference was not found in both specimens. As can be seen in Fig. 9, excluding r_b at the small deformation, r_b abruptly increased with the elastic-limit of unbonded tendons at the negative loading. On the other hand, r_b at the positive loading remained almost zero, regardless of the elastic-limit of tendons. Because of the slab reinforcement and the following decrease of λ, the residual beam deflection greatly increased at the negative loading, as can be seen in Fig. 4. Accordingly, the residual deflection, at the positive loading, began to move toward the origin point, and the flexural behavior at the positive and the negative loading became totally different. The ratio r_b at the maximum story shear force ($Q_{max,avg}$: average of $\pm Q_{max}$) in both specimens was zero and ranged from 0.24 to 0.31, at the positive and the negative loading, respectively.

The values of r_b at the positive and the negative loading were estimated from Eq. (2), which is one of proposed methods to predict r_b (=r/R_P) in the reference [2], and they are plotted by dashed lines together with experiment results (Fig. 9). In specimen PCJ02S herein, the prestress ratio (λ) which is the same value with specimen PCJ01S (λ=0.59) was employed at its negative loading, since the cut-offed slab reinforcing bars were found to considerably contribute to the flexural behavior. The prediction results of r_b could almost approximate the test results at the negative loading, excluding the early stage of loadings, but they highly overestimated those results at the positive loading. Hence, the evaluation method should consider the effect of λ in a T-shaped beam with unbonded tendons, which simultaneously changes at the positive and the negative loading.

$$r = 0.3(1.1-\lambda)\cdot(R_p \times 100)^{(3+\lambda)/2}/100 \tag{2}$$

where, r is the residual beam deflection angle at the unloading stage, R_p is the beam deflection angle at the peak loading and λ is the prestress ratio.

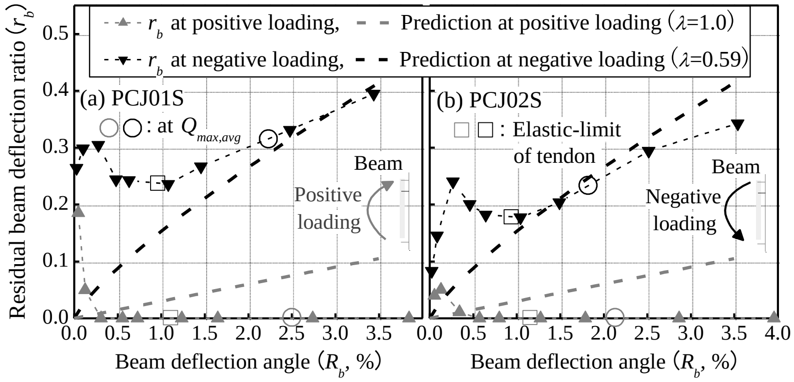

Fig. 9 – Residual beam deflection ratio-beam deflection angle relation (Avg. value in west and east beams)

4.4 Residual crack opening width at beam-column interface

The residual crack opening width (w_{max}) at the beam-column interface was investigated when the beam shear force became zero at the unloading stage. The relation between w_{max} and the beam deflection angle (R_b), recorded at each peak loading, is shown in Fig. 10. In this study, the experiment data obtained from the displacement transducers, attached adjacent to beam-column interfaces (50mm apart from column and beam faces), was interpolated, and the opening distance at the extreme tension fiber was employed for w_{max}. The values of w_{max} were likely to increase sharply after the elastic-limit of tendons at the negative loading, but those of positive loading were found almost zero, which had almost similar tendency with the residual beam deflection ratio (r_b). The width w_{max} at the maximum story shear force in both specimens were found 0mm and 1.6 to 2.2mm at the positive and the negative loading, respectively.

The prediction results of w_{max} are also plotted in Fig. 10, which were obtained from Eq. (3) in the reference [2]. It should be noted that Eq. (3) is to estimate the maximum residual crack width of a beam member, but it was applied to evaluate the crack opening width (w_{max}) at the beam-column interface in this paper. In the equation, the proposed value of n_f for a RC member is 2, which also indicates the equivalent numbers of flexural cracks developing at either the top or the bottom side of the beam, but 1 was employed for n_f herein, because the crack width is likely to concentrate on beam critical sections in an unbonded PCaPC beam. As can be seen in Fig. 10, the estimated w_{max} showed good correspondence with the experiments at the negative loading, as was found in r_b of Fig. 9, but they did not correspond with those results at the positive loading.

$$w_{\max} = \alpha(D - x_n)r / n_f \tag{3}$$

where, n_f is the ratio of the maximum residual crack width to the sum of total flexural crack widths (set 1.0), α is the ratio of flexural deformation to total deformation of a beam (set 1.0), D is the beam depth, x_n is the distance from the compression fiber to the neutral axis (set approximate value of 0.1D and 0.2D at the positive and the negative loading, respectively, from Fig. 8(a)) and r is the value from Eq. (2).

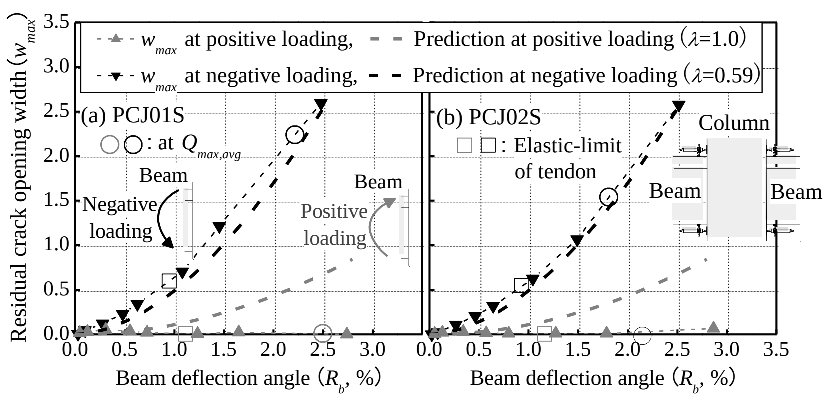

Fig. 10 – Residual crack opening width-beam deflection angle relation (Avg. value in west and east beams)

4.5 Energy dissipating capacity of beam member

The equivalent viscous damping ratio (h_{eq}) was calculated to investigate the energy dissipating capacity of unbonded PCaPC beams. The second loading cycles of experiment results were used to obtain h_{eq}, and the relation between h_{eq} and the beam deflection angle (R_b), at each peak loading, is shown in Fig. 11. Herein, h_{eq} was computed at the positive and the negative loading, respectively, since each beam shear force-beam deflection relation was significantly different. As expected, h_{eq} at the negative loading was higher than that of the positive loading due to the slab reinforcement. The ratio h_{eq} was slightly higher in specimen PCJ01S, since its residual deflection was relatively larger. The cut-offed slab bars in specimen PCJ02S is also considered to be one of factors affecting the energy dissipating capacity. With the yielding of the slab reinforcement, h_{eq} tended to gradually increase at the negative loading; however, that of the positive loading was likely to be nearly constant

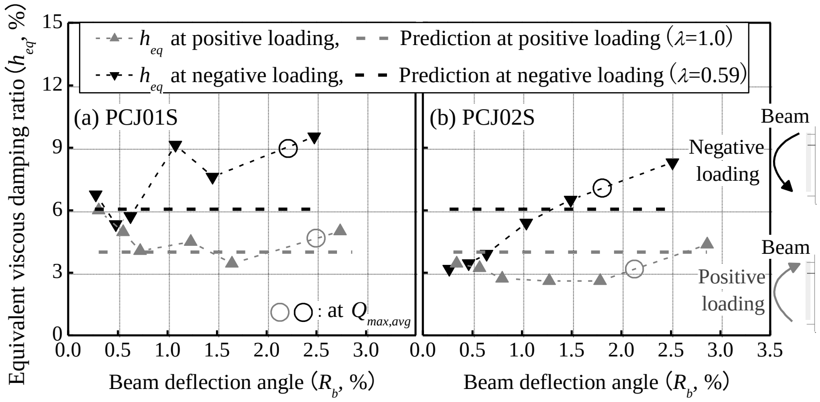

Fig. 11 – Equivalent viscous damping ratio-beam deflection angle relation (Avg. in west and east beams)

before the maximum strength. In both specimens, h_{eq} at the positive and the negative loading was about 3 to 5% and 7 to 9%, respectively, at their maximum story shear force.

Dashed lines in Fig. 11 are the prediction results of h_{eq} at the positive and the negative loading. Herein, h_{eq} was calculated from the reference [5] considering the bond condition along the tendon and the prestress ratio (λ), which is also one of the evaluation methods adopted in the reference [2]. In this evaluation method, for a beam having unbonded tendons and no beam longitudinal bars passing through the joint, the value of h_{eq} is supposed to be constant according to λ. As shown in Fig. 11, the estimated h_{eq} at the negative loading was likely to underestimate the test result with the increase of beam deformation, although it was not a large discrepancy. Hence, the effect of the slab reinforcement in a T-shaped beam with unbonded tendons, on h_{eq} at the negative loading, should be considered in the prediction method. In contrast, the evaluation result of h_{eq} at the positive loading could almost approximate the experiment result with a slight overestimation; also, the tendency which remained nearly constant was well reproduced.

4.6 Different limit states of beam

The reference [2] from the Architectural Institute of Japan has proposed a recommendation determining the limit state of a prestressed concrete beam as four-levels as shown in Table 3, which is to be applicable to a beam member with unbonded tendons. The limit states consist of 'service limit state', 'fist restorable limit state', 'second restorable limit state' and 'safety limit state'. They are decided from the damage conditions of the beam

Table 3 – Recommendation of damage factor and level to determine different limit states of beam[2]

Different limit state	Damage factor and level							
	Range of prestress ratio (λ)	Ordinary bar	Prestressing tendon		Concrete		Residual deflection angle	Residual crack width
			Good bond	Poor bond	Usual flexural member	Other members*3)		
Service limit state	1~0.75	Permission of slight yielding	Elastic range	Elastic range	Less than 0.9σ_B*2)	Less than 0.75σ_B	Nearly Zero	Less than 0.2mm
	0.75~0.5		Less than σ_y*1)		Less than (14/15λ+0.2)σ_B			
	Less than 0.5	Elastic range			Less than 2/3σ_B			
First restorable limit state	Permission of yielding		Permission of slight yielding	Elastic range	Slight crushing of cover concrete		Less than 1/400	Less than 1.0mm
Second restorable limit state	No buckling of longitudinal bar		Permission of yielding	Less than σ_y	Severe crushing of cover concrete		Less than 1/200	Less than 2.0mm
Safety limit state	No rupture of longitudinal bar		No rupture	Permission of yielding	No crushing of core concrete		Upper limit of deflection angle (4%)	

*1) Yield strength determined by 0.2% offset method
*2) Concrete compressive strength
*3) A member having distinctive axial load as external force

Table 4 – Damage factor and level for each different limit state & corresponding beam deflection (West beam)

Damage factor and level \ Specimen		PCJ01S		PCJ02S	
		At negative Load.	At positive Load.	At negative Load.	At positive Load.
Slab bar	Slight yielding (Yielding)	0.26(●)	－	0.34(●)	－
	Buckling	－	－	－	－
	Rupture	－	－	－	－
Prestressing tendon	Elastic-limit	0.99(▲)	1.08(▲)	0.94(▲)	1.14(▲)
	Slight yielding (Yielding)	－	－	－	－
Concrete	Slight cover concrete crushing	1.07(△)	1.71(△)	1.47(△)	1.78(△)
	Severe cover concrete crushing	2.44(▽)	2.73(▼)	2.56	2.85(▼)
	Core concrete crushing	3.40(□)	－	3.63(□)	－
Residual deflection angle	1/400 (0.25%)	1.06(△)	－	1.29(△)	－
	1/200 (0.5%)	1.72(▼)	－	1.95(▼)	－
Residual crack width	0.2mm	0.42(○)	－	0.45(○)	－
	1.0mm	1.30(△)	－	1.42(△)	－
	2.0mm	2.04(▽)	－	2.12 (▽)	－
Upper limit of deflection angle (R_b)		4.0 (□)	4.0 (□)	4.0 (□)	4.0 (□)
Damage factor & level which determined each limit state	Service limit state	Slab bar yielding (0.26%)	－	Slab bar yielding (0.34%)	－
	First restorable limit state	Elastic-limit of tendon (0.99%)	Elastic-limit of tendon (1.08%)	Elastic-limit of tendon (0.94%)	Elastic-limit of tendon (1.14%)
	Second restorable limit state	Residual Def. angle of 1/200 (1.72%)	Severe cover Con. crushing (2.73%)	Residual Def. angle of 1/200 (1.95%)	Severe cover Con. crushing (2.85%)
	Safety limit state	Core concrete crushing (3.40%)	Upper limit of R_b (4.0%)	Core concrete crushing (3.63%)	Upper limit of R_b (4.0%)

* ○・△・▽・□ are possible factors determining 'Service limit state'・'First restorable limit state'・'Second restorable limit state'・'Safety limit state', respectively, and ●・▲・▼・■ are the factors which determined those limit states.

* －: No data・N.A

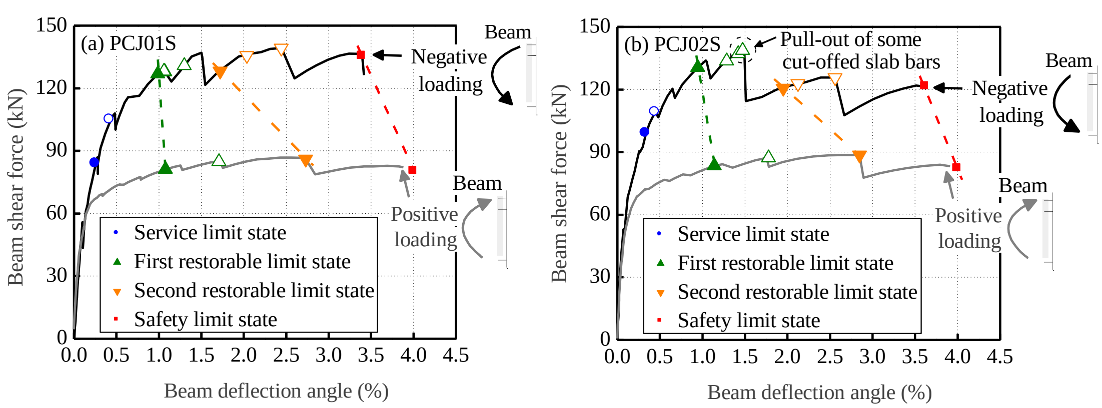

Fig. 12 – Different limit state on envelope of beam shear force-beam deflection angle relation (West beam)

reinforcement, the tendon and the concrete, as well as from the residual deflection angle and the residual crack width. In Table 3, the slight yielding of the reinforcement and the tendon was set to be their yielding points from the material tests. It should be noted that, in this study, the criteria for the beam longitudinal bar (ordinary bar) was substituted for the slab reinforcement (Table 4), since the beam longitudinal reinforcement was terminated at the beam-column face in the unbonded PCaPC beam of this study. The specified value of the concrete compressive stress, indicated in Table 3, was not taken into account in this paper, because it was somewhat difficult to figure out from the experiment. When the beam cover concrete either had compressive cracks along its axial direction or spalled off slightly, it was regarded as the slight crushing of cover concrete in Table 3. The spall-off of cover concrete, extending almost through the entire beam width, was set to be cover concrete crushing. After the cover concrete crushing, if the reinforcing bar was exposed, it was assumed core concrete crushing. It should be also noted that the beam deflection angle, for the criteria of the residual deflection angle and the residual crack width in Table 3, was interpolated from the beam deflection angles having the values close to those criterial values. The damage factors which decided each different limit state and the corresponding beam deflection angles are summarized in Table 4. Fig. 12 shows the envelope curves of beam shear force (Q_b)-deflection angle (R_b) relations in both specimens, at their positive and negative loading, together with the results of Table 4. The point which determined each limit state is also plotted, and those points with same limit states are mutually connected in the figure.

At the negative loading in both specimens, the 'service limit state' was determined from the initiation of slab bar yielding, which preceded the residual maximum crack width of 0.2mm. The elastic-limit of unbonded tendons, which decided the 'first restorable limit state', occurred before the slight crushing of cover concrete and the residual maximum crack with of 1mm. After the elastic-limit of unbonded tendons, the residual deflection ratio abruptly increased as mention earlier, so the 'second restorable limit state' was determined from the criterion of the residual deflection angle (1/200). Finally, the core concrete crushing was the factor deciding the 'safety limit state' of the beam. The 'service limit state' decided by the initiation of slab bar yielding, which was obtained from 0.2% offset method, did not well reflect the stiffness degradation point on the backbone curve (Fig. 12). The 'first restorable limit state' determined from the elastic-limit of unbonded tendons agreed approximately with the stiffness degradation point on the envelope curve, but the 'second restorable limit state' by the residual deflection angle of 1/200 did not well reflect the strength deterioration point in specimen PCJ01S with no cut-offed slab reinforcement.

On the other hand, at the positive loading, there is only one criterion to determine the 'service limit state', which is the residual crack width of 0.2mm, for the unbonded PCaPC beam of this study, because beam longitudinal bars were terminated at the column face and precise values of the concrete compressive stress were not easy to acquire from the experiment. Moreover, the crack width exceeding 0.2mm was not observed, since the prestress ratio (λ) at the positive loading was 1.0 and that of the negative loading was somewhat low; hence, no 'service limit state' was found at the positive loading. The residual deflection was considerably slight at the positive loading, as mentioned earlier, so the 'first restorable limit state' was determined from the elastic-limit of unbonded tendons. Also, because unbonded tendons are unlikely to yield, the 'second restorable limit state' was decided by cover concrete crushing, which showed good correspondence with the strength deterioration point (Fig. 12). When a positive load applies to a T-shaped beam, the distance (x_n) from the extreme compression fiber to the neutral axis becomes smaller than that of a negative loading (Fig. 8), so concrete damage at the top of beam critical sections was somewhat lesser than that of the bottom. As a result, the 'safety limit state' was determined from the upper limit of the beam deflection angle (4%, which was an arbitrarily decided value). As mentioned above, there was no clear point to determine the 'service limit state' of the beam, so the stiffness degradation was not faithfully reproduced in the specimens. In addition, in the case of an unbonded PCaPC beam, the residual deflection and the residual crack width could be minor due to the high value of λ, as was found in this experiment. Based on these results, it is considered that more reasonable criteria for an unbonded PCaPC member, having λ of 1.0, should be investigated in the future study.

The beam deflection angles at the 'service limit state', which only existed at the negative loading, were 0.26 to 0.34%, and those of the 'fist restorable limit state' were 0.94 to 1.14%. At the 'second restorable limit state', the beam deflection angles ranged from 1.72 to 2.85%, which showed a huge difference according to loading directions. Those angles at the 'safety limit state' were found 3.40 to 4.0%, and the concrete damage was found relatively severe at the bottom of beam critical sections.

5. Conclusions

The precast prestressed concrete subassemblages, assembled by post-tensioning unbonded tendons, with cast-in-place RC slabs were tested under reversed cyclic loading, and the following conclusions were drawn:

(1) Slightly lesser cracks developed in the RC slab of the specimen, which had partial cut-off of slab reinforcement; however, the crack patterns of the slabs in both specimens did not show distinctive difference due to the development length of the cut-offed slab bars. Regardless of the partial cut-off of the slab reinforcement,

the effective slab width exceeded 0.1 and 0.2 times the beam span at beam deflection angles of 0.4% and 1.2%, respectively. Also, almost whole slab width contributed to the flexural capacity of a T-shaped beam at the end of the test in the specimen having no cut-offed slab bars.

(2) Because of the slab reinforcement and the different prestress ratio, the flexural behavior of a T-shaped beam with unbonded tendons was found totally different at its positive and negative loading. The beam shear force-beam deflection angle relation showed origin-oriented hysteresis loops at the positive loading, having the prestress ratio of 1.0, while that of the negative loading exhibited fat spindle-shaped loops due to the yielding of slab bars.

(3) The maximum values of the residual beam deflection ratio and the residual crack opening width were found about 0.4 and 2.5mm, respectively, at the negative loading, when the prestress ratio was about 0.59. However, the residual beam deflection and the residual crack opening were almost zero at the positive loading, with the prestress ratio of 1.0.

(4) In a T-shaped beam with unbonded tendons, the equivalent viscous damping ratio at the positive loading tended to become nearly constant. In contrast, the equivalent viscous damping ratio at the negative loading gradually increased with the yielding of the slab reinforcement, and it was almost two times larger than that of the positive loading at the maximum strength.

(5) The predicted values of the residual beam deflection ratio and the residual crack opening width, based on a new guideline from the Architectural Institute of Japan, well agreed with experiment results at the negative loading. On the other hand, the equivalent viscous damping ratio estimated from the guideline showed good correspondence with that of test results at the positive loading. Therefore, more prospective studies should be conducted on those evaluation methods.

(6) Elastic-limit of unbonded tendons and severe crushing of cover concrete could approximately reproduce the stiffeness and the strength degrading point on the backbone curve. At the positive loading of an unbonded PCaPC beam with the prestress ratio of 1.0, there are few factors which can determine its service limit state, due to little residual deflection and the termination of beam longitudinal bars at the column face; therefore, more reasonable criteria should be investigated in the future study. The concrete damage was found relatively severe at the bottom of beam critical sections, because of the larger distance from the compression fiber to the neutral axis at the negative loading, which led to the safety limit state.

6. Acknowledgements

The financial support of the Association for Sustainable Building Systems (ASBS) from Japanese Ministry of Land, Infrastructure, Transport and Tourism is gratefully appreciated.

7. References

[1] Stanton J, Stone WC, Cheok GS (1997): A Hybrid Reinforced Precast Frame for Seismic Regions, *PCI journal*, **42**(2), 20-32.

[2] AIJ (2015), Guidelines for Structural Design and Construction of Prestressed Concrete Buildings based on Performance Evaluation Concept (Draft), Architectural Institute of Japan. (in Japanese)

[3] Shiohara H, Kusuhara F (2012): Joint Shear? or Column-to-Beam Strength Ratio? Which is a key parameter for seismic design of RC Beam-column joints-Test Series on Interior Joints, *Proceedings of 15th World Conference on Earthquake Engineering*, Lisbon, Portugal, September

[4] Shima T, Kitayama K, Endo T (2014): Seismic Performance and Different Limit States of Prestressed Reinforced Concrete Frame with Slab Dominated by Beam Flexural Behavior, *Proceedings of the Japan Concrete Institute*, **Vol.36**, No.2, 727-732. (in Japanese)

[5] Tajima Y, Kitayama K (2012): Estimation of Equivalent Viscous Damping Ratio for Flexural Beam in Prestressed Reinforced Concrete Frame, *Proceedings of 15th World Conference on Earthquake Engineering*, Lisbon, Portugal, September.